# TAZ, a Transcriptional Modulator of Mesenchymal Stem Cell Differentiation

Jeong-Ho Hong,[1] Eun Sook Hwang,[3] Michael T. McManus,[1] Adam Amsterdam,[1] Yu Tian,[4] Ralitsa Kalmukova,[1] Elisabetta Mueller,[5] Thomas Benjamin,[4] Bruce M. Spiegelman,[5] Phillip A. Sharp,[1] Nancy Hopkins,[1] Michael B. Yaffe[1,2]*

Mesenchymal stem cells (MSCs) are a pluripotent cell type that can differentiate into several distinct lineages. Two key transcription factors, Runx2 and peroxisome proliferator–activated receptor γ (PPARγ), drive MSCs to differentiate into either osteoblasts or adipocytes, respectively. How these two transcription factors are regulated in order to specify these alternate cell fates remains a pivotal question. Here we report that a 14-3-3–binding protein, TAZ (transcriptional coactivator with PDZ-binding motif), coactivates Runx2-dependent gene transcription while repressing PPARγ-dependent gene transcription. By modulating TAZ expression in model cell lines, mouse embryonic fibroblasts, and primary MSCs in culture and in zebrafish in vivo, we observed alterations in osteogenic versus adipogenic potential. These results indicate that TAZ functions as a molecular rheostat that modulates MSC differentiation.

Pluripotent MSCs can differentiate into several distinct cell types, including osteoblasts and adipocytes (*1*, *2*). Two key transcription factors, Runx2 (also called Cbfa1 or Pebp2αA) and PPARγ, drive MSCs to differentiate into either osteoblasts or adipocytes, respectively (*3*–*7*), and the differentiation of each lineage appears to be mutually exclusive and transcriptionally controlled (*8*, *9*). How these two transcription factors are regulated in order to specify these alternate cell fates is unknown.

The balance between MSC osteoblast and adipocyte differentiation is disrupted in various human diseases. For example, decreased bone formation accompanied by an increase in bone marrow adipogenesis occurs with aging and immobility or following corticosteroid use (*10*–*14*), whereas increased bone formation is observed in patients with progressive osseous hyperplasia who form heterotopic bone within their adipose tissue (*15*). In addition, MSCs are currently being explored as vehicles for cell-based skeletal therapies (*16*, *17*). Therefore, investigating the

[1]Center for Cancer Research, Department of Biology and [2]Division of Biological Engineering, Massachusetts Institute of Technology, 77 Massachusetts Avenue, E18-580, Cambridge, MA 02139, USA. [3]Department of Immunology and Infectious Diseases, Harvard School of Public Health, Harvard Medical School, Boston, MA 02115, USA. [4]Department of Pathology, Harvard Medical School, 77 Louis Pasteur Avenue, Boston, MA 02115, USA. [5]Dana-Farber Cancer Institute and the Department of Cell Biology, Harvard Medical School, Boston, MA 02115, USA.

*To whom correspondence should be addressed. E-mail: myaffe@mit.edu

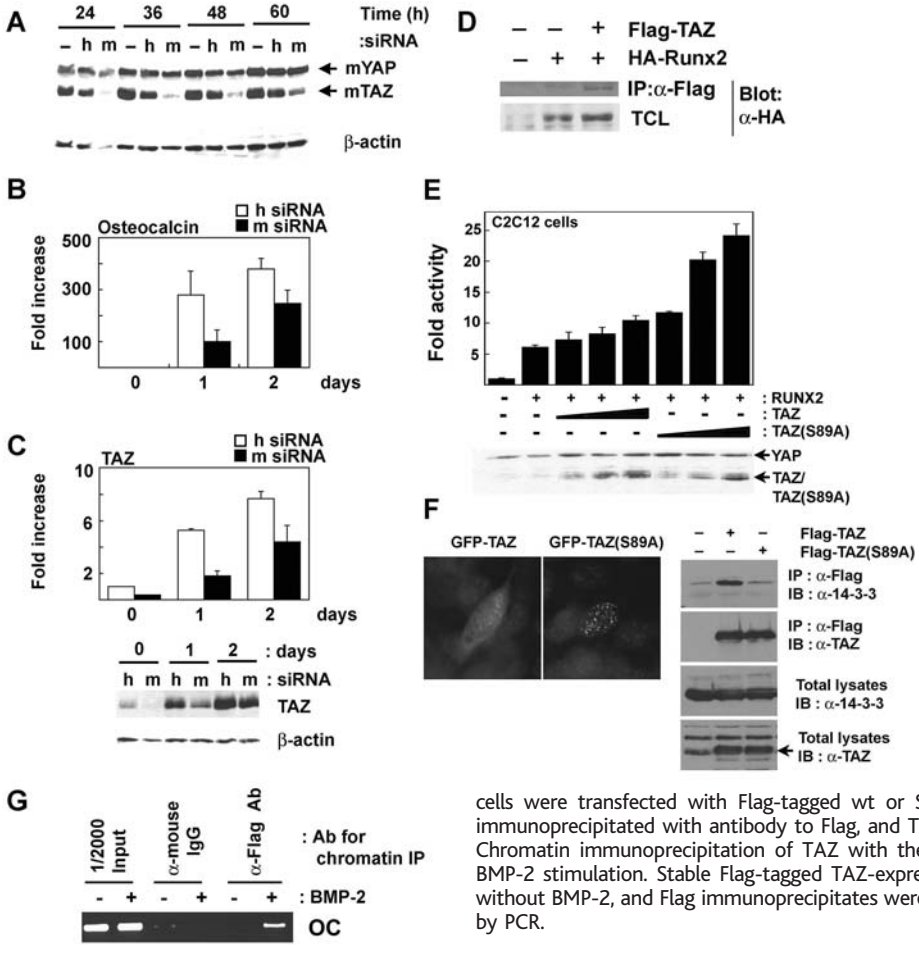


**Fig. 1.** TAZ is a Runx2 transcriptional coactivator for osteocalcin expression. (**A**) Down-regulation of TAZ by siRNA. Murine (m) and human (h) TAZ siRNA duplex oligonucleotides were transfected into murine C2C12 cells, and lysates were analyzed by immunoblotting (*18*). (**B**) Decreased octeocalcin expression after down-regulation of endogenous TAZ. Total RNA was prepared and osteocalcin gene expression at the indicated times after BMP-2 treatment was quantified by using real-time polymerase chain reaction (PCR) and normalized to β-actin expression. (**C**) TAZ expression in response to BMP-2. RNA and cell lysates from (B) were analyzed for TAZ mRNA expression by real-time PCR (upper panel) and for protein expression by Western blot analysis (lower panel). (**D**) Direct interaction between TAZ and Runx2. 293T cells were transfected with Flag-tagged TAZ, HA-tagged Runx2, or both, and total cell lysates (TCL) were analyzed by coimmunoprecipitation. (**E**) Stimulation of Runx2-driven gene expression by TAZ. Luciferase reporter activity from a construct containing six copies of the Runx2-binding site in the osteocalcin promoter was measured in cell lysates 24 hours after transfection and normalized to β-galactosidase activity. Below is a Western blot analysis of TAZ (wild-type or S89A) and YAP levels in the lysates. (**F**) 14-3-3 binding and nuclear localization of TAZ S89A mutant protein. (Left) Green fluorescent protein (GFP)–tagged TAZ wild-type and S89A localization in transfected C2C12 cells. (Right) C2C12 cells were transfected with Flag-tagged wt or S89A mutant TAZ. Protein from total lysates was immunoprecipitated with antibody to Flag, and TAZ or 14-3-3 was detected by immunoblotting. (**G**) Chromatin immunoprecipitation of TAZ with the endogenous osteocalcin promoter in response to BMP-2 stimulation. Stable Flag-tagged TAZ-expressing C2C12 cells were treated for 3 days with or without BMP-2, and Flag immunoprecipitates were analyzed for osteocalcin (OC) promoter occupancy by PCR.

mechanisms that fine-tune the balance between MSC osteoblast and adipocyte differentiation is likely to be of medical importance.

TAZ is a paralog (related molecule arising in a single species through gene duplication) of Yes-associated protein (YAP) that we identified in a proteomic screen for 14-3-3–binding proteins (*18*). The function of TAZ is unknown, although it can act as a transcriptional coactivator when overexpressed (*18*, *19*). TAZ and YAP contain a WW domain that binds to Pro-Pro-X-Tyr motifs (where X is any amino acid) and a coiled-coil C-terminal domain that recruits core components of the transcriptional machinery (*18*, *20*). A number of transcription factors including Runx2 and PPARγ contain Pro-Pro-X-Tyr motifs within their activation domains. Thus, interaction of TAZ with these and other transcription factors might be involved in mediating their transcriptional effects.

To investigate the function of TAZ, we designed small interfering RNAs (siRNAs) against the murine (m) or human (h) TAZ isoforms (fig. S1). These siRNAs differ at two base pairs and function as specific and nonspecific control siRNAs in mouse and human cell culture, respectively. The murine-specific TAZ siRNA, but not the human-specific siRNA, decreased the abundance of TAZ protein within 24 hours when transfected into murine myoblast C2C12 cells (Fig. 1A). Neither siRNA had any effect on YAP expression. Treatment of C2C12 cells with bone morphogenic protein–2 (BMP-2) induces osteoblast differentiation as evidenced by an ~400-fold increase in Runx2-dependent expression of the osteocalcin gene, a late marker of osteoblast development (*21*, *22*). Transfection of C2C12 cells with murine TAZ siRNA for 24 hours before exposure to BMP-2 inhibited osteocalcin gene expression relative to the effect of the human TAZ siRNA (Fig. 1B). BMP-2 treatment itself caused a 10- to 20-fold increase in the expression of both TAZ mRNA and protein over the ensuing 2 days in these cells, an effect that was blunted, but not eliminated, by siRNA treatment (Fig. 1C).

Thus, BMP-2 appears to stimulate a transcriptional program in which increased expression of TAZ, as well as subsequent TAZ-stimulated expression of the osteocalcin gene by Runx2, may be important for the osteoblast differentiation program. To test this idea, we performed immunoprecipitation experiments and verified a direct interaction of TAZ and Runx2 in transfected cells (Fig. 1D). TAZ expression caused a dose-dependent increase in Runx2-driven expression of an osteocalcin gene promoter fragment construct monitored in a luciferase reporter assay (Fig. 1E and fig. S2). 14-3-3 binds to TAZ through a site involving $Ser^{89}$, sequestering TAZ in the cytoplasm and limiting its ability to influence gene expression (*18*). Replacement of $Ser^{89}$ with Ala (S89A mutation) disrupted 14-3-3 binding and relocalized TAZ preferentially within the nucleus, often in punctate foci (Fig. 1F) (*18*). When we used an S89A mutant of TAZ, the TAZ-dependent transcriptional coactivation of Runx2-driven gene expression was enhanced 2 to 3 times (Fig. 1E). Similar results for Runx2 transcriptional coactivation were obtained in C3H10T1/2 mouse embryonic fibroblasts (fig. S3). Both the interaction of TAZ with Runx2 and the stimulatory effect of TAZ on osteocalcin gene promoter activity were dependent on the TAZ WW domain (fig. S7). We also generated stable C2C12 cell lines expressing Flag-tagged TAZ and observed a BMP-2–dependent targeting of TAZ to the endogenous osteocalcin promoter by chromatin immunoprecipitation. (Fig. 1G). Taken together, these data indicate that TAZ is a 14-3-3–regulated transcriptional coactivator for

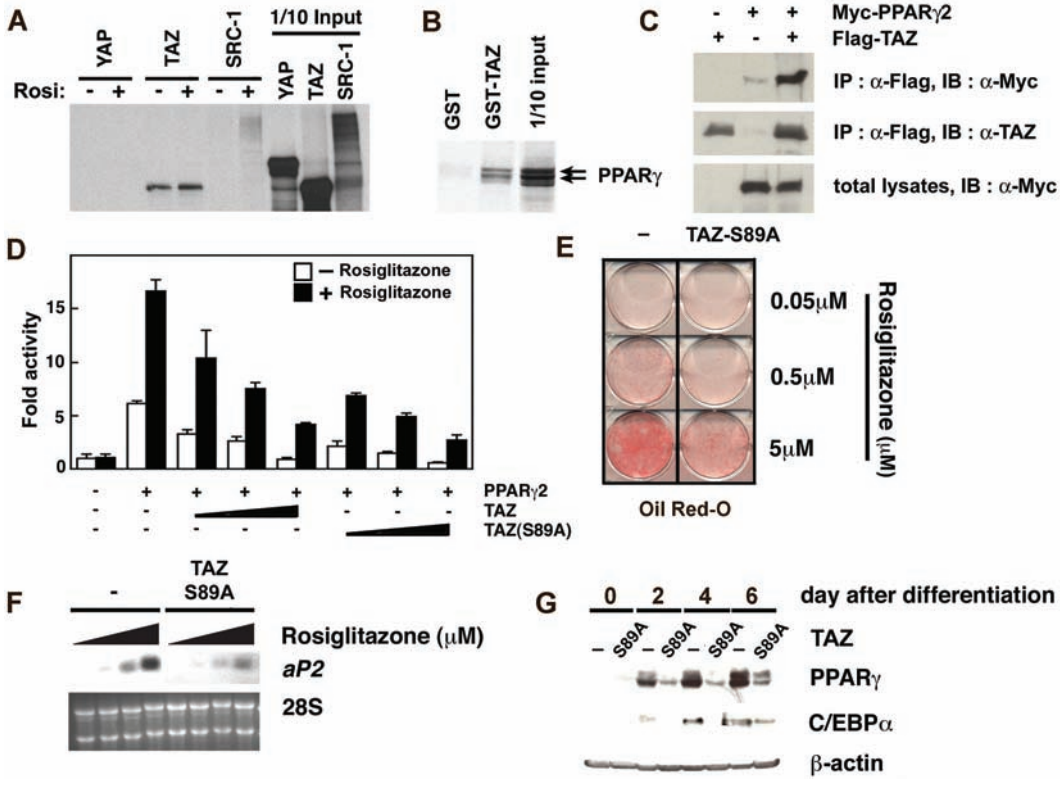


**Fig. 2.** TAZ binds to PPARγ and inhibits transcription from the aP2 promoter. (**A**) Binding of TAZ to glutathione *S*-transferase (GST) fused with PPARγ. Immobilized GST-PPARγ was incubated with in vitro translated, $^{35}$S-labeled YAP or TAZ, or with the ligand-dependent PPARγ-binding protein SRC-1, in the presence or absence of 1 μM Rosiglitazone, and analyzed by autoradiography. (**B**) Binding of PPARγ to GST-TAZ. Immobilized GST-mTAZ was incubated with in vitro translated $^{35}$S-labeled PPARγ. The PPARγ doublet represents sites of alternative translational initiation. (**C**) Interaction of TAZ with PPARγ in cells. 293T cells were transfected with Flag-tagged TAZ or Myc-tagged PPARγ and analyzed by coimmunoprecipitation. (**D**) Inhibition of PPARγ-driven gene expression by TAZ. U2OS cells were transfected with an aP2 promoter–containing firefly luciferase reporter construct (aP2-Luc), a PPARγ expression vector [SV-sport–PPARγ2, (*6*)] and various amounts of plasmids encoding either wt-TAZ or the S89A TAZ mutant (EF-mTAZ-NFLAG or EF-mTAZ(S89A)-NFLAG, respectively). Total DNA in each sample was equalized by addition of empty pEF-Bos vector DNA. Luciferase activity was measured after 24 hours in the presence or absence of 1 μM Rosiglitazone and normalized to the activity of a cotransfected *Renilla* luciferase reporter construct used as an internal control. (**E**) Inhibition of adipocyte differentiation by stable expression of TAZ. 3T3-L1 cells were infected with a control pBabe-puro retroviral vector (–) or a retroviral vector containing TAZ S89A. Puromycin-resistant cells were treated with Rosiglitazone and stained with Oil Red O and photographed at 8 days (*6*). (**F**) Expression of fatty acid–binding protein aP2. Total RNA was isolated from cells in (E), and probed with an adipocyte-specific cDNA to aP2. Ethidium bromide staining (bottom) verifies equal loading of RNA in each lane. (**G**) Inhibition of PPARγ-dependent gene expression by TAZ S89A. Retrovirally infected cells were lysed at the indicated times after treatment with 5 μM Rosiglitazone, and PPARγ and C/EBPα protein levels were analyzed by Western blotting.

Runx2-stimulated osteocalcin gene expression and an important endogenous regulator of osteoblast differentiation.

PPARγ, a member of the nuclear hormone receptor superfamily, is a ligand-activated transcription factor that is critical for adipocyte differentiation (*6*, *7*, *9*, *23*–*25*). Like Runx2, PPARγ also contains a Pro-Pro-X-Tyr WW domain–binding motif within its ligand-independent activation domain. We therefore investigated the functional interaction between TAZ and PPARγ. PPARγ bound in a ligand-independent manner to TAZ, but not to YAP, in experiments with tagged proteins in vitro and in transfected cells (Fig. 2A through C). In contrast to the stimulatory effect of TAZ on Runx2-driven gene expression, TAZ directly inhibited the ability of PPARγ to stimulate gene expression for the endogenous fatty acid–binding protein aP2, in both the presence and absence of the PPARγ-activating ligand Rosiglitazone, as assayed with a luciferase reporter construct (Fig. 2D). The inhibitory effect of TAZ on PPARγ-driven gene expression was even more pronounced when the constitutively nuclear S89A form of TAZ was used (Fig. 2D). Similar to what we observed with Runx2, the interaction of TAZ with PPARγ and the inhibitory effect of TAZ on aP2 gene expression required the TAZ WW domain (fig. S8).

To investigate the cellular role of TAZ on PPARγ-regulated genes, we generated stable 3T3-L1 cell lines expressing TAZ-S89A or a vector control, and we monitored adipocyte differentiation in response to Rosiglitazone. Enhanced expression of TAZ-S89A resulted in inhibition of adipocyte differentiation as revealed by suppression of Rosiglitazone-induced expression of aP2 and reduction in Oil Red O staining of the cells (Fig. 2, E and F). PPARγ participates in a positive feedback loop by driving transcription of its own gene, as well as that of other target genes such as the one for C/EBPα, as part of the normal adipocyte differentiation program (*26*). Overexpression of TAZ-S89A also inhibited these PPARγ-driven processes (Fig. 2G). Similar results were also observed with wild-type TAZ, although its effect was smaller. TAZ did not affect binding of PPARγ to its site on the aP2 promoter as seen from an oligonucleotide-binding assay (fig. S9). Instead, chromatin immunoprecipitation experiments localized TAZ to the endogenous aP2 promoter during these adipocyte differentiation experiments (Fig. 3D). Thus, TAZ may suppress adipocyte differentiation by transcriptionally repressing PPARγ-driven gene expression.

To further examine this possibility, we used siRNA to inhibit the production of endogenous TAZ in this same cell type (Fig. 3). After TAZ was depleted, the 3T3-L1 cells were placed in adipocyte differentiation medium containing various concentrations of Rosiglitazone. Cells were assayed 8 days later, by which

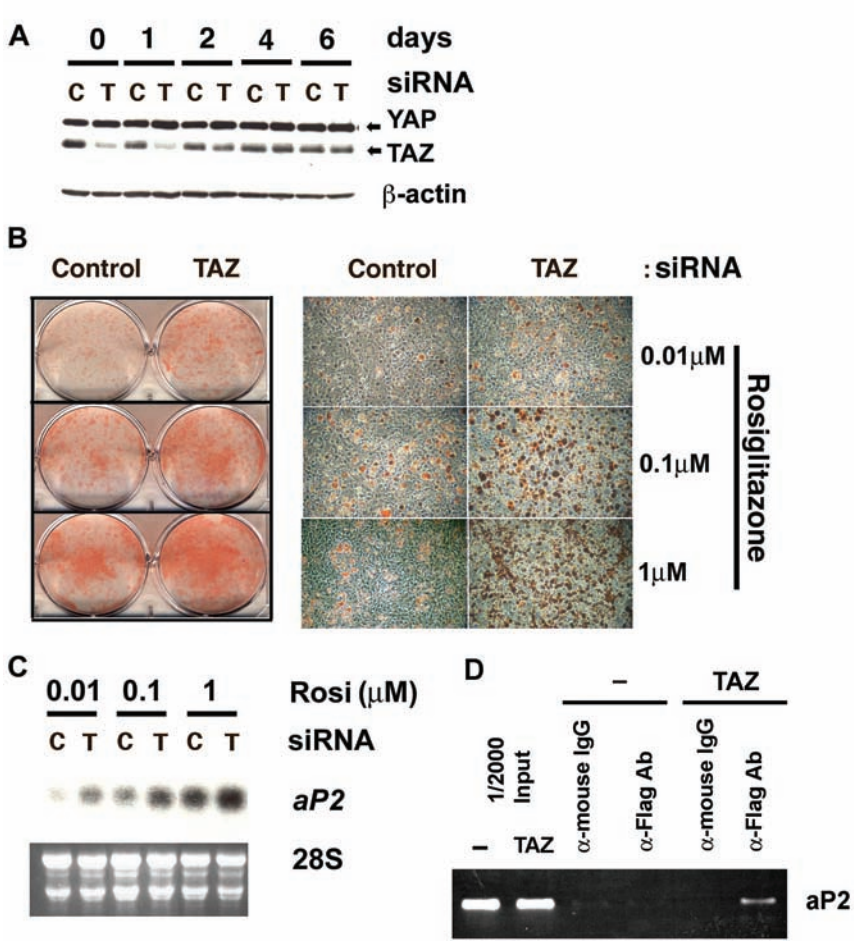


**Fig. 3.** Increased adipocyte differentiation from cells depleted of endogenous TAZ. (**A**) 3T3-L1 cells were transfected with control siRNA against GFP (C) or mTAZ-specific siRNA (T) for 36 hours and transferred to adipocyte differentiation medium. Cell lysates were examined for TAZ and YAP expression by Western blotting. (**B**) Adipogenesis in cells after inhibition of endogenous TAZ expression. As in (A), 3T3-L1 cells were treated with the indicated concentrations of Rosiglitazone for 8 days, stained with Oil Red O, and photographed. (**C**) Total RNA was isolated from cells shown in (B) and probed with an adipocyte-specific cDNA to aP2. (**D**) Stable 3T3-L1 cells expressing pBabe-puro retroviral vector control (–) or Flag-tagged wild-type TAZ were differentiated into adipocytes and analyzed by chromatin immunoprecipitation with the use of PCR primers for the endogenous aP2 promoter.

time TAZ expression was no longer inhibited. However, the transient reduction of expression of endogenous TAZ was sufficient to enhance ligand-induced adipocyte differentiation at each concentration of Rosiglitazone tested (Fig. 3, A through C). We conclude that TAZ is a transcriptional repressor of PPARγ-induced gene expression and an endogenous inhibitor of the adipocyte differentiation program.

Osteoblasts and adipocytes originate from the same MSCs through alternative activation of reciprocal transcriptional programs (*8*, *9*). Our findings suggested that TAZ may influence cell fate during the MSC differentiation process, because Runx2, PPARγ, and TAZ are present in these cells (Fig. 4, A and B; fig. S4). To test this, we isolated primary MSCs from murine bone marrow, allowed them to proliferate in culture, and infected them with control retroviruses or with retroviruses encoding short hairpin RNAs (shRNAs) against TAZ. Retrovirus-infected cells were selected after 7 days of culture in medium containing puromycin, and the entire surviving population of cells was assayed. Using this approach, we observed an ~75% reduction in TAZ protein expression (Fig. 4B). When these cells were subsequently cultured under conditions favoring osteoblast differentiation, the cells infected with the control retrovirus showed calcium deposition by 5 days (Fig. 4, C and D). In contrast, cells infected with the retroviruses encoding shRNAs against TAZ demonstrated almost no calcium deposition at this time, which revealed impairment of the osteoblast differentiation program. Conversely, when retrovirus-infected primary MSCs were cultured under conditions favoring adipocyte differentiation, the cells containing shRNA against TAZ demonstrated enhanced Oil Red O staining (Fig. 4E).

We wondered whether the increased adipogenic phenotype observed in cells lacking TAZ was blunted by the waning effectiveness and limited suppression of TAZ resulting from expression of siRNA or shRNA, respectively. We

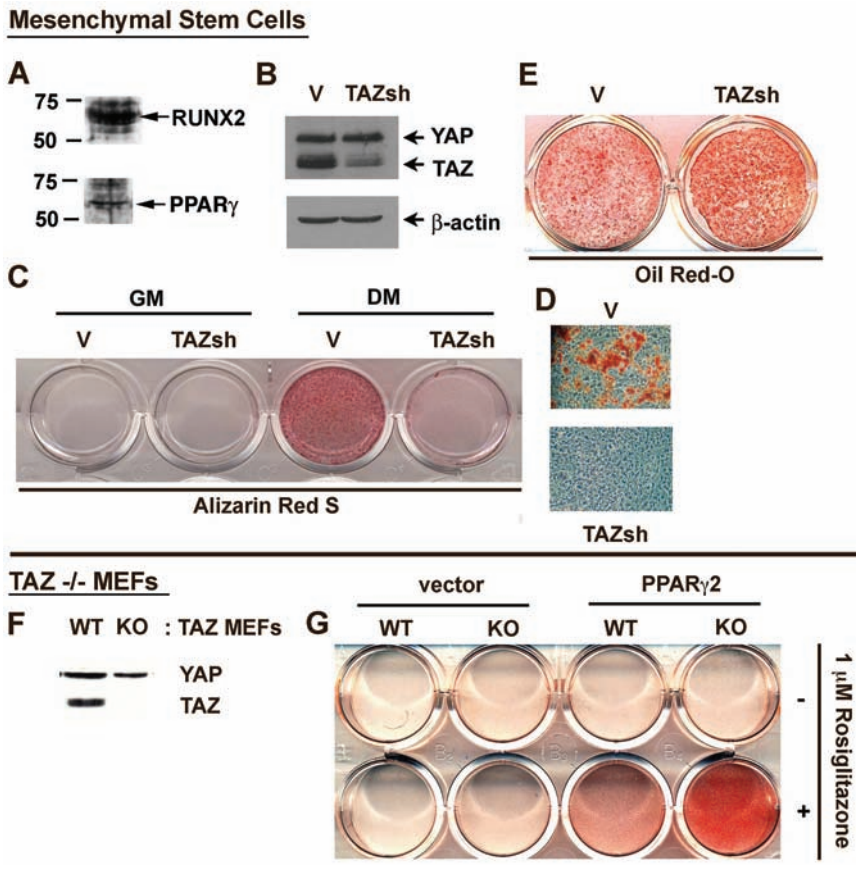


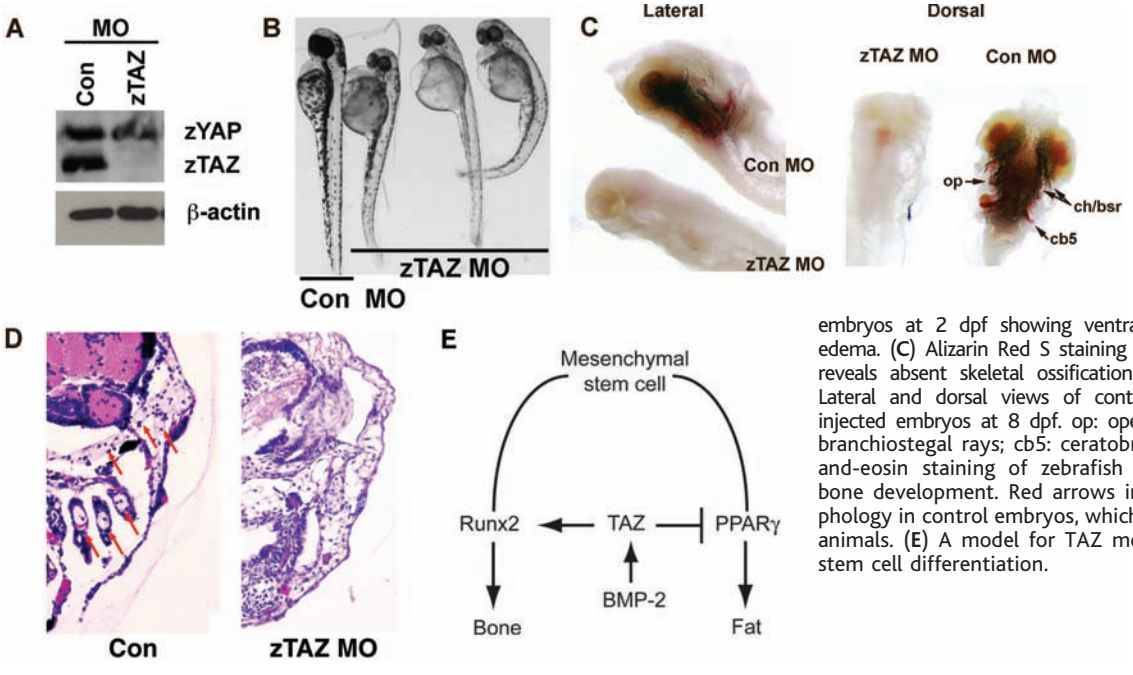


**Fig. 4.** Bone marrow-derived MSCs depleted of TAZ show decreased osteogenesis and increased adipogenesis. (**A**) Concurrent expression of Runx2 and PPARγ in primary bone marrow–derived MSCs. Nuclear extracts from MSCs were analyzed by Western blotting with the indicated antibodies. (**B**) Depletion of TAZ with shRNA. MSCs were infected with a pSRP retrovirus control (V) or pSRP encoding TAZ short hairpin RNA (TAZsh). After puromycin selection for 7 days, the MSC population was analyzed for depletion of endogenous TAZ by Western blotting. (**C** and **D**) Impaired osteoblast differentiation TAZ-depleted MSCs. After 7 days of selection in puromycin, amplified cells were transferred to medium containing 0.1 μM dexamethasone, 50 μg/ml ascorbic acid, and 10 mM β-glycerophosphate for 5 days to induce osteoblast differentiation. Plates were stained with Alizarin Red S to visualize intracellular calcium deposition and photographed. (**E**) Enhanced adipocyte differentiation in TAZ-depleted MSCs. MSCs were induced to differentiate into adipocytes by culture in medium containing 1 μM dexamethasone, 5 μg/ml insulin, and 1 μM Rosiglitazone for 8 days, stained with Oil Red O, and photographed. (**F**) TAZ expression in knockout MEFs. TAZ expression was analyzed in whole-cell lysates from wild-type and $TAZ^{-/-}$ MEFs by using an antibody that recognizes both TAZ and YAP. (**G**) Enhanced adipocyte differentiation of TAZ knockout MEFs. Wild-type and $TAZ^{-/-}$ MEFs were infected with a PPARγ2-expressing retrovirus or a retrovirus vector control, and the infected cells were selected by using puromycin. Cells were induced with differentiation medium in the presence or absence of 1 μM Rosiglitazone as above, stained with Oil Red O, and photographed.

**Fig. 5.** Lack of skeletal ossification in TAZ-depleted zebrafish. (**A**) TAZ depletion in zebrafish embryos. Embryos were injected with a control morpholino oligomer (MO) or a TAZ-specific oligomer at the one- to two-cell stage and analyzed 1 to 2 days later by immunoblotting. (**B**) Morphology of TAZ-depleted zebrafish embryos at 2 dpf showing ventral curvature and pericardial edema. (**C**) Alizarin Red S staining of whole zebrafish embryos reveals absent skeletal ossification in TAZ-depleted embryos. Lateral and dorsal views of control- and TAZ-specific MO-injected embryos at 8 dpf. op: opercle; ch/bsr: ceratohyal and branchiostegal rays; cb5: ceratobranchial. (**D**) Hematoxylin-and-eosin staining of zebrafish sections reveals impaired bone development. Red arrows indicate normal bone morphology in control embryos, which is absent in TAZ-depleted animals. (**E**) A model for TAZ modulation of mesenchymal stem cell differentiation.

therefore addressed adipocyte differentiation in wild-type mouse embryo fibroblasts (MEFs) and $TAZ^{-/-}$ MEFs generated by homologous recombination (*27*) (Fig. 4F). MEFs were immortalized, infected with a retrovirus expressing PPARγ2, and cultured in medium containing Rosiglitazone to induce adipogenesis. Adipogenesis was more pronounced in $TAZ^{-/-}$ MEFs than in wild-type cells (Fig. 4G and fig. S5), consistent with a negative role of endogenous TAZ in the adipocyte differentiation process.

To investigate the in vivo role of TAZ on bone development, we used a zebrafish vertebrate model system. We cloned the zebrafish TAZ ortholog (fig. S6) and used antisense morpholino oligomers injected at the one- to two-cell stage to decrease expression of TAZ (Fig. 5A). The TAZ-depleted embryos survived for up to 8 days after fertilization (dpf), and had developmental abnormalities including a ventral axis curvature and pericardial edema

(*28*) (Fig. 5B). Bone development was visualized in whole embryos by Alizarin Red S staining (Fig. 5C), along with hematoxylin-and-eosin staining of thin sections (Fig. 5D). In control animals, extensive skeletal development was evident in the cranial and pharyngeal region at 8 dpf. No bone formation was observed in any of the TAZ-depleted embryos at 8 dpf, the latest time point we could observe before embryonic death. These findings confirm a critical role for TAZ in osteoblast differentiation in vivo. We are unable to comment on the role of TAZ in adipogenesis in these embryos, because adipocytes have not been described in teleosts (although they presumably exist), and in other vertebrate species, fat deposition does not occur until the postnatal period (*23*).

One function of TAZ is as a transcriptional modifier of mesenchymal stem cell differentiation by promoting osteoblast differentiation while simultaneously impairing adipocyte differentiation, as we have shown (Fig. 5E). Differentiation of MSCs into osteoblasts is critically dependent on Runx2 (*4*, *5*). Our findings implicate TAZ in this process: (i) TAZ functions as an endogenous coactivator of Runx2 in cells; (ii) stimuli that promote bone formation transcriptionally up-regulate TAZ concurrently with Runx2; and (iii) TAZ-deficient zebrafish embryos are defective in bone formation. In contrast, stem cell differentiation into adipocytes requires PPARγ-dependent transcriptional events that are directly inhibited by endogenous TAZ. Thus, TAZ may act as a molecular rheostat to fine-tune the balance between osteoblast and adipocyte development.

### References and Notes


1. M. F. Pittenger *et al.*, *Science* **284**, 143 (1999).
2. A. I. Caplan, S. P. Bruder, *Trends Mol. Med.* **7**, 259 (2001).
3. P. Ducy, R. Zhang, V. Geoffroy, A. L. Ridall, G. Karsenty, *Cell* **89**, 747 (1997).
4. T. Komori *et al.*, *Cell* **89**, 755 (1997).
5. F. Otto *et al.*, *Cell* **89**, 765 (1997).
6. P. Tontonoz, E. Hu, B. M. Spiegelman, *Cell* **79**, 1147 (1994).
7. E. D. Rosen *et al.*, *Mol. Cell* **4**, 611 (1999).
8. K. Nakashima, B. de Crombrugghe, *Trends Genet.* **19**, 458 (2003).
9. E. D. Rosen, C. J. Walkey, P. Puigserver, B. M. Spiegelman, *Genes Dev.* **14**, 1293 (2000).
10. P. Meunier, J. Aaron, C. Edouard, G. Vignon, *Clin. Orthop.* **80**, 147 (1971).
11. R. Burkhardt *et al.*, *Bone* **8**, 157 (1987).
12. O. Kajkenova *et al.*, *J. Bone Miner. Res.* **12**, 1772 (1997).
13. S. Verma, J. H. Rajaratnam, J. Denton, J. A. Hoyland, R. J. Byers, *J. Clin. Pathol.* **55**, 693 (2002).
14. M. E. Nuttall, J. M. Gimble, *Bone* **27**, 177 (2000).
15. F. S. Kaplan, E. M. Shore, *J. Bone Miner. Res.* **15**, 2084 (2000).
16. D. J. Prockop, *Science* **276**, 71 (1997).
17. S. C. Chang *et al.*, *J. Surg. Res.* **119**, 85 (2004).
18. F. Kanai *et al.*, *EMBO J.* **19**, 6778 (2000).
19. C. B. Cui, L. F. Cooper, X. Yang, G. Karsenty, I. Aukhil, *Mol. Cell. Biol.* **23**, 1004 (2003).
20. R. Yagi, L. F. Chen, K. Shigesada, Y. Murakami, Y. Ito, *EMBO J.* **18**, 2551 (1999).
21. T. Katagiri *et al.*, *J. Cell Biol.* **127**, 1755 (1994).
22. S. Gallea *et al.*, *Bone* **28**, 491 (2001).
23. P. Cornelius, O. A. MacDougald, M. D. Lane, *Annu. Rev. Nutr.* **14**, 99 (1994).
24. Y. Barak *et al.*, *Mol. Cell* **4**, 585 (1999).
25. N. Kubota *et al.*, *Mol. Cell* **4**, 597 (1999).
26. Z. Wu *et al.*, *Mol. Cell* **3**, 151 (1999).
27. Y. Tian, T. Benjamin, unpublished observations.
28. J.-H. Hong, N. Hopkins, M.B. Yaffe, unpublished observations.


29. Assistance from H. Jo and R. Nissen in zebrafish studies and S. Bissonnette in MSC studies is gratefully acknowledged. This work was supported by NIH grants CA042063 to P.A.S., and GM60594 and GM68762 and a Burroughs-Wellcome Career Development Award to M.B.Y.


**Supporting Online Material**

www.sciencemag.org/cgi/content/full/309/5737/1074/DC1
Materials and Methods
Figs. S1 to S9
References and Notes


11 February 2005; accepted 28 June 2005
10.1126/science.1110955


# Formation of Regulatory Patterns During Signal Propagation in a Mammalian Cellular Network


**Avi Ma'ayan,[1] Sherry L. Jenkins,[1] Susana Neves,[1] Anthony Hasseldine,[1] Elizabeth Grace,[1] Benjamin Dubin-Thaler,[3] Narat J. Eungdamrong,[1] Gehzi Weng,[1]* Prahlad T. Ram,[1]† J. Jeremy Rice,[4] Aaron Kershenbaum,[4] Gustavo A. Stolovitzky,[4] Robert D. Blitzer,[1,2] Ravi Iyengar[1]‡**



**We developed a model of 545 components (nodes) and 1259 interactions representing signaling pathways and cellular machines in the hippocampal CA1 neuron. Using graph theory methods, we analyzed ligand-induced signal flow through the system. Specification of input and output nodes allowed us to identify functional modules. Networking resulted in the emergence of regulatory motifs, such as positive and negative feedback and feedforward loops, that process information. Key regulators of plasticity were highly connected nodes required for the formation of regulatory motifs, indicating the potential importance of such motifs in determining cellular choices between homeostasis and plasticity.**


A mammalian cell may be considered as a central signaling network connected to various cellular machines that are responsible for phenotypic functions (*1*). Cellular machines such as transcriptional, translational, motility, and secretory machinery can be represented as sets of interacting components that form functional local networks. The central signaling network that connects the various machine networks also receives and processes signals from extracellular entities such as hormones or neurotransmitters and ions. Experimental work has defined how different pathways interact to form networks and small-scale regulatory configurations such as switches (*2*, *3*), gates (*4*, *5*), feedback loops (*6*, *7*), and feedforward motifs (*8*, *9*) that decode signal duration and strength and process information. Identifying and characterizing regulatory motifs can move us from thinking about individual components to considering the functions of groups of components that act in a coordinated manner. Understanding how the functional organization of cellular systems changes in response to information flow is an important goal in systems biology. For systems containing many components, obtaining an overview of the patterns of regulatory motifs and defining their interrelationships can provide a format for in-depth analysis of individual units using quantitative biochemical representations.

From data in the experimental literature, we constructed a system of interacting cellular components involved in phenotypic behavior and used graph theory methods (*10*–*12*) to analyze qualitative relationships between nodes (components) in a network. In signaling networks, activation is achieved as a response to a stimulus. Information propagates through the system by a series of coupled biochemical reactions to regulate components responsible for cellular phenotypic functions. Here, we identify the regulatory features that emerge during such information flow in a simplified representation of a mammalian hippocampal CA1 neuron. Such neurons are capable of plasticity as defined by their ability to undergo long-term potentiation of synaptic responses (*13*, *14*).

We represented the CA1 neuron as a set of interacting components that make up a network of signaling pathways that connects to various


Departments of [1]Pharmacology and Biological Chemistry and [2]Psychiatry, Mount Sinai School of Medicine, New York, NY 10029, USA. [3]Department of Biological Sciences, Columbia University, New York, NY 10029, USA. [4]Functional Genomics and Systems Biology, IBM T. J. Watson Research Center, Yorktown Heights, NY 10598, USA.

*Present address: Scios Inc., 6500 Paseo Padre Parkway, Fremont, CA 94555, USA.
†Present address: Department of Molecular Therapeutics, M. D. Anderson Cancer Center, Houston, TX 77025, USA.
‡To whom correspondence should be addressed. E-mail: Ravi.Iyengar@mssm.edu